ACS APPLIED ELECTRONIC MATERIALS

pubs.acs.org/acsaelm Forum Article

Thickness-Dependent Magnetism and Topological Properties of $EuSn_2As_2$

Xiaodong Lv,[⊥] Xuejiao Chen,[⊥] Bingwen Zhang, Peiheng Jiang,* and Zhicheng Zhong*

Cite This: *ACS Appl. Electron. Mater.* 2022, 4, 3212−3219 Read Online

ACCESS | Metrics & More | Article Recommendations | Supporting Information

ABSTRACT: Rare-earth magnetic compounds, known as conventional magnetic materials and magnetic topological materials, provide a platform for exploring prominent physics phenomena and designing topological spintronic devices. $EuSn_2As_2$, as a candidate of intrinsic antiferromagnetic (AFM) topological insulator, has recently attracted considerable attention in experiment. Here, by using density functional theory to systematically investigate the structure, magnetic, electronic, and topological properties, we demonstrate that the interlayer coupling, magnetic order, and spin orientation strongly influence the electronic and topological properties of $EuSn_2As_2$. The $EuSn_2As_2$ monolayer (1L) is a topological trivial ferromagnetic semiconductor. Increasing the thickness can lead to the appearance of interlayer AFM in the 2L and insulator to metal transition in the 3L one, respectively. Moreover, the nontrivial surface states that resulted from the band inversion between Sn p and As p orbitals can be obtained in the 4L one. Our study reveals the spin textured band effect, i.e., spin-orientation-controlled band structure effect, in $EuSn_2As_2$, and also evidence the importance of dimensional effect for the electronic properties and magnetic behaviors of this material as van der Waals AFM topological insulators.

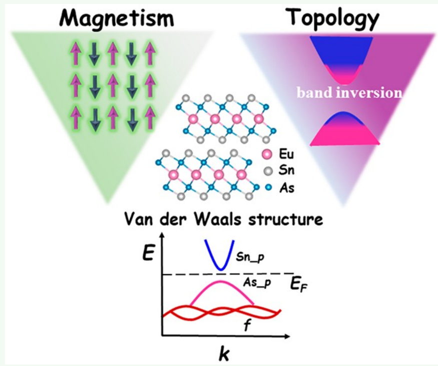

KEYWORDS: *rare-earth magnetic compounds, spin textured band effect, electronic and topological properties, band inversion, dimensional effect*

■ INTRODUCTION

The materials with magnetic and topological nontrivial bands can give rise to many forefront electronic states, such as magnetic Weyl/Dirac semi-metals,[1,2] high-order topological insulators (TIs),[3] and antiferromagnetic (AFM) TIs.[4,5] These novel electronic states have promising applications for designing next-generation spintronic devices[6] so that it motivates enormous interest searching for more intrinsically magnetic topological materials.[7−9] Recently, several materials, including the $MnBi_2Te_4$ family,[10] Mn_3X (X = Sn, Ge, Ir),[11] Co_2YZ (Y = V, Zr, Nb, Ti, Hf; Z = Si, Ge, Sn),[12] $Co_3Sn_2S_2$,[13] and so on, have been verified to exhibit a fascinating magnetic topological state. Their magnetic topological phase can be further tuned by various of manipulation techniques, e.g., rotating the magnetic moment orientation,[14−17] doping,[18] strain,[19] dimensional tuning,[20] etc. Hence, the discovery of the intrinsic magnetic topological materials and effective manipulation of their magnetic topological phase are crucial for achieving exotic magnetic topological quantum phenomena.

$MnBi_2Te_4$ is discovered to be a typical van der Waals (vdW) magnetic topological material. It exhibits intralayer ferromagnetic (FM) and interlayer AFM order, i.e., A-type AFM order. Bulk $MnBi_2Te_4$ is an AFM insulator with axion state,[21] while the density functional theory (DFT) calculation indicates that the FM $MnBi_2Te_4$ is a topological Weyl semi-metal (WSM).[22] The vdW $MnBi_2Te_4$ also exhibits thickness-dependent topological behavior. The monolayer one is a topological trivial FM semiconductor, while its multilayers host the states of quantum anomalous Hall (QAH) for even layers and zero plateau QAH for odd layers.[20]

Except for the known $MnBi_2Te_4$ system, the thickness-dependent magnetism and electronic properties are also reported in other vdW systems. For example, the FM Weyl semi-metal Co_2MnGa exhibits a thickness-dependent anomalous Hall effect,[23] the layered topological superconductor β-$PdBi_2$ shows thickness-dependent superconductivity,[24] and the magnetic ground state of 1T-CrT_2 is also highly dependent on the film thickness.[25] Although several works have been focused on these kinds of materials, the materials with tunable intrinsic magnetic topological properties are still rare.

Recently, a new family of vdW Eu-based magnetic compounds (EuM_2X_2, M = In, Sn and X = P, As),[26−29] which share similar crystal structure with $MnBi_2Te_4$, has been

Special Issue: 2D Magnetism - Materials, Devices, and Applications

Received: March 31, 2022
Accepted: May 24, 2022
Published: June 7, 2022

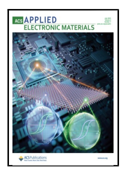

https://doi.org/10.1021/acsaelm.2c00414
ACS Appl. Electron. Mater. 2022, 4, 3212−3219

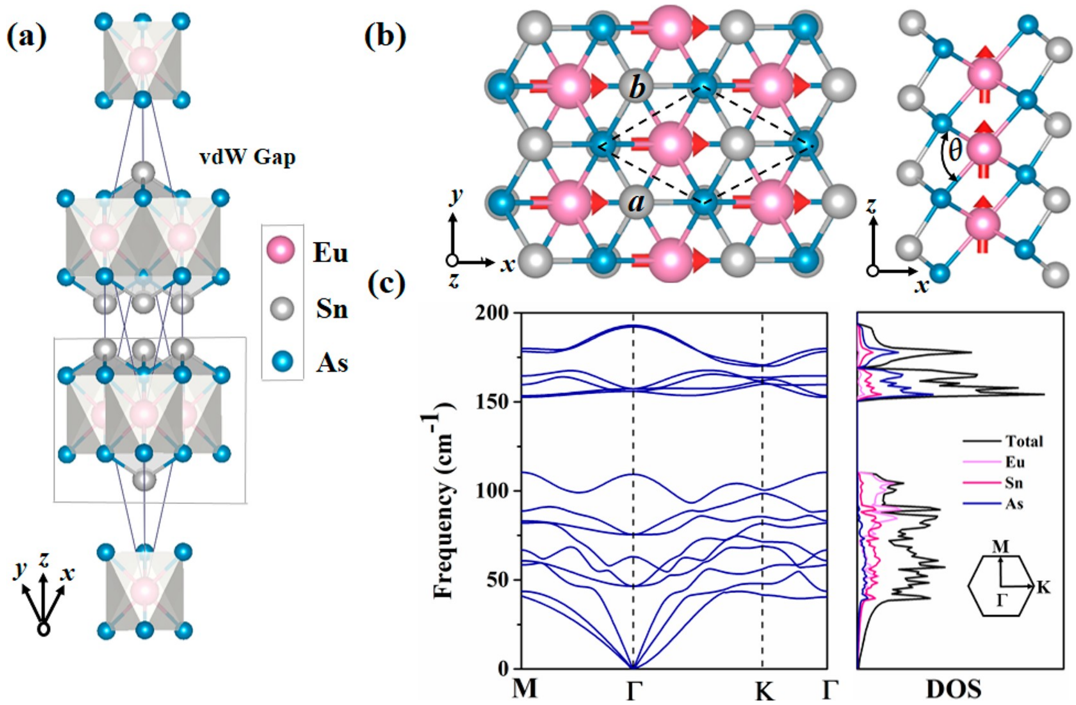

Figure 1. (a) Crystal structures of the bulk $EuSn_2As_2$. The solid line stands for the single layer. (b) Top and side views of $EuSn_2As_2$ monolayer. Dashed lines indicate the unit cell. The pink, blue, and gray balls represent the Eu, As, and Sn atoms, respectively. The red arrows stand for the direction of the spin moments. (c) Phonon dispersion and corresponding density of states of $EuSn_2As_2$ monolayer. Inset is the Brillouin zone.

suggested to be a promising candidate of AFM topological insulator. In this family, $EuSn_2As_2$ is one of the few intrinsic magnetic topological insulators that has been theoretically predicted and experimentally confirmed. $EuSn_2As_2$ undergoes a paramagnetic (PM) to AFM phase transition at 24 K.[30] The magnetic order is A-type AFM which is the same with $MnBi_2Te_4$.[31,32] Angle-resolved photoemission spectroscopy (ARPES) combined with DFT calculations prove that $EuSn_2As_2$ is an AFM TI with no observed gap in Dirac surface at low temperature and there exists a transition from strong TI (Z_2 = 1) to axion insulator (Z_4 = 2) following the magnetic transition from PM to AFM phase.[33] However, the previous studies mainly focus on the magnetic structure and quantum transport properties of bulk $EuSn_2As_2$; systematic research on the interplay among magnetism, electronic, and topological properties and their thickness dependence is still missing.

In this work, we report a comprehensive study on the structure, magnetic, electronic, and topological properties of monolayer and multilayer $EuSn_2As_2$ by means of first-principles calculations. Our calculations reveal that the ground state of $EuSn_2As_2$ monolayer holds FM order with an in-plane easy axis, and it is a topological trivial FM semiconductor with an indirect band gap of 0.60 eV. An indirect−direct band gap transition can be tuned by switching the spin orientation from in-plane to out-of-plane. Remarkably, the $EuSn_2As_2$ thin films can achieve semiconductor−metal transition in three layers (denoted as 3L) and topological surface states in 4L. Our work thus not only demonstrates the dimensional-dependent magnetism and electronic properties in $EuSn_2As_2$ but also provides an effective magnetism and topology tuning strategy in these vdW layered materials.

COMPUTATIONAL METHODS

The calculations were performed within DFT as implemented in the Vienna ab initio simulation package (VASP).[34] The generalized gradient approximation (GGA) in the form of the Perdew−Burke−Ernzerhof (PBE)[35] exchange−correlation functional was employed. The core electrons were treated using the projector augmented wave (PAW) method.[36] The plane-wave cutoff energy was set to be 500 eV. A vacuum space of 15 Å was adopted to avoid interactions between periodical slabs. The DFT-D2 approach was used to describe the vdW interactions.[37] The Brillouin zone was sampled with the Monkhorst−Pack scheme[38] by 9 × 9 × 1 and 14 × 14 × 1 *k*-meshes for crystal structure relaxation and electronic structure calculations, respectively. The structures were fully relaxed until the energy and force are less than 10^{-5} eV and 10^{-4} eV/Å, respectively. The spin−orbit coupling (SOC) is included in electronic structure calculations. The strong on-site Coulomb repulsion of Eu f electrons were described with the GGA+*U* scheme with a value of U = 5 eV.[39] The phonon spectrum calculated with the PHONOPY code[40] on the basis of density functional perturbation theory (DFPT) was adopted to evaluate the dynamical stability of $EnSn_2As_2$ monolayer. The ab initio molecular dynamics (AIMD) simulations were carried out to investigate the thermal stability, with the temperature being controlled by the Nosé−Hoover method.[41] The Monte Carlo (MC) simulations[42] based on the classical Heisenberg model with magnetic anisotropy energies (MAEs) and exchange coupling constant, J,[43] are performed to estimate the critical temperature.

RESULTS AND DISCUSSION

A. Crystal Structures of $EnSn_2As_2$. Figure 1a shows the crystal structure of bulk $EnSn_2As_2$. It shares a similar structure and the same space group of $R\bar{3}m$ with $MnBi_2Te_4$, so that it also exhibits vdW layered character with honeycomb SnAs layers and a trigonal Eu layer stacked alternatively. The vertical distance between adjacent layers is d_0 = 2.37 Å (Supporting Information Figure S1a). The calculated lattice constants, Sn/Eu−As bond lengths, and Eu−As−Eu bond angles are listed in

https://doi.org/10.1021/acsaelm.2c00414
ACS Appl. Electron. Mater. 2022, 4, 3212−3219

Table 1. Calculated Lattice Constant, *a* or *b* (Å), Sn−/Eu−As Bond Lengths, d_{Sn-As} and d_{Eu-As} (Å), Angle of the Eu−As−Eu bond, $\angle_{Eu-As-Eu}$ (deg), Magnetic Ground States Energy Differences, Δ*E*, MAE (meV/Eu), and Band Gaps of $EuSn_2As_2$ with different thicknesses[a]

thickness	*a*(*b*)	d_{Sn-As}	d_{Eu-As}	$\angle_{Eu-As-Eu}$	order	Δ*E*	MAE	gap
1L	4.17	2.78	3.11	84.17	FM	164.9	0.05	0.60
2L	4.19	2.79	3.10	84.89	cAFM	−1.14	0.03	0.13
3L	4.20	2.79	3.11	85.29	uAFM	−0.83	1.66	metal
4L	4.21	2.80	3.10	85.19	cAFM	−4.96	0.50	metal
5L	4.23	2.81	3.14	84.87	uAFM	−0.37	−0.06	metal
6L	4.23	2.82	3.14	84.85	cAFM	−1.22	0.45	metal
7L	4.25	2.82	3.13	85.45	uAFM	−0.01	2.29	metal
8L	4.25	2.81	3.14	85.20	cAFM	−1.67	−0.53	metal
bulk	4.24	2.82	3.14	85.25	uAFM	−1.17	0.04	metal
exp[31]	4.21	2.78	3.10	85.40	uAFM			metal

[a]The energy difference, Δ*E* (meV/Eu), is defined as $(E_{AFM\_out\text{-}of\text{-}plane} - E_{FM\_out\text{-}of\text{-}plane})/n$ with *n* being the number of Eu atoms. cAFM and uAFM stand for the compensated and uncompensated AFM states, respectively.

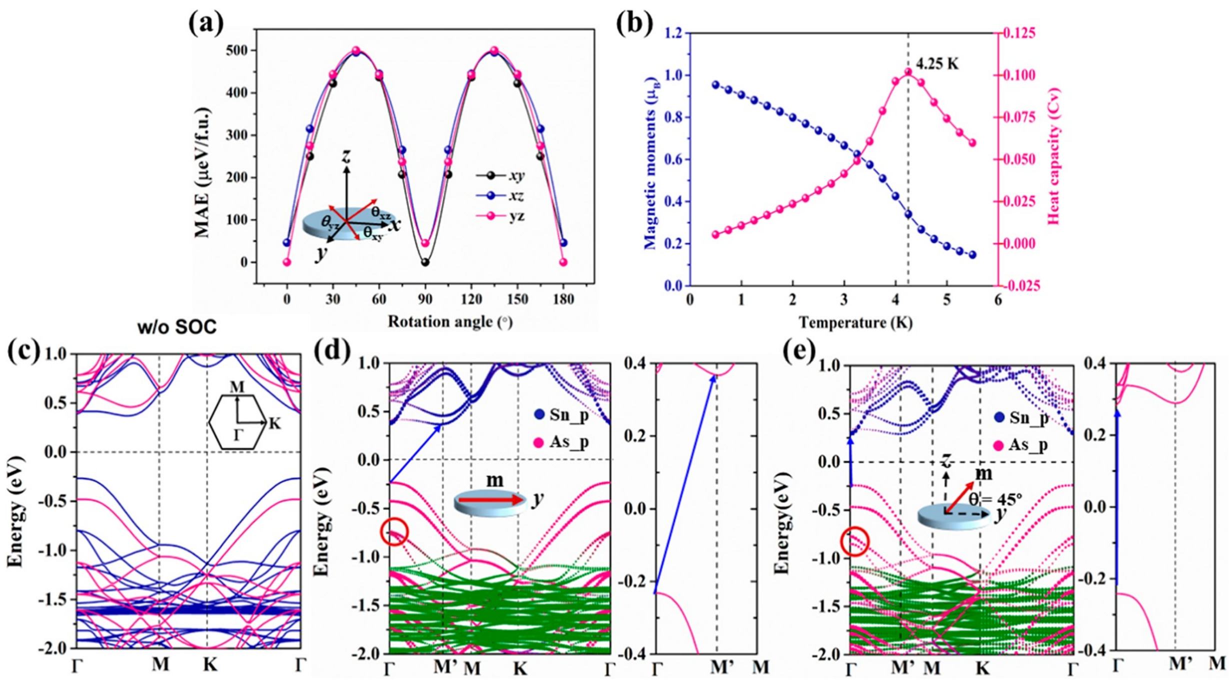

Figure 2. (a) MAE of $EnSn_2As_2$ monolayer with magnetic direction, varying in *xy*/*xz*/*yz* planes. (b) Variation of the average normalized magnetic moment (*M*) associated with the specific heat (C_v) as a function of the temperature for the $EnSn_2As_2$ monolayer. (c−e) Atom-orbital-resolved band structures of $EnSn_2As_2$ monolayer with different magnetic configurations: (c) FM configurations without SOC and spin orientation along (d) (010) and (e) (011) directions with inclusion of SOC. The blue cyan and pink curves express the spin-up and spin-down bands, and the green curves represent the Eu f bands.

Table 1. The magnetic calculations show that intralayer Eu atoms are FM coupled and interlayer ones AFM coupled, i.e., A-type AFM order, which is in the same order with $MnBi_2Te_4$ and is also in good agreement with the experimental results.[31]

To demonstrate the structure character of these vdW materials, we first focus on $EuSn_2As_2$ monolayer as shown in Figure 1b. The structure of the monolayer belongs to the space group of *Pmmn*. It exhibits a honeycomb lattice from the top view and consists of five atomic layers with the sequence of Sn−As−Eu−As−Sn from the side view. In detail, one Eu layer is sandwiched between two Sn−As layers, in which each Eu atom bonds with six neighboring As atoms and each Sn atom bonds three As atoms, forming a $SnAs_3$ tetrahedron. The relaxed in-plane lattice parameters are found to be *a* = *b* = 4.17 Å, which is 1.6% smaller than the bulk value (4.24 Å). Consequently, this leads to a shorter Sn−As bond length, which suggests a stronger chemical bonding in monolayer as confirmed in Figure S1d.

To investigate the fabrication efficient of this vdW material, we calculate the cleavage energy of 1L from a 5L thick slab (approximated to the bulk; see Figure S1a). The calculated cleavage energy of the monolayer $EnSn_2As_2$ is 43.72 meV/Å^2, which is in the typical range for layered compounds, indicating that the $EnSn_2As_2$ monolayer is experimentally feasible.[44] The stability of the $EnSn_2As_2$ monolayer is further comprehensively verified by several schemes. The dynamic stability of $EnSn_2As_2$ monolayer is evaluated by calculating the phonon spectra as shown in Figure 1c; the absence of imaginary phonon modes confirms that it is dynamically stable. The thermal stability at high temperature is assessed by performing AIMD simulations. Neither bond breakage nor structure distortion can be noted at 800 K, and the monolayer can maintain its structural integrity,

https://doi.org/10.1021/acsaelm.2c00414
ACS Appl. Electron. Mater. 2022, 4, 3212−3219

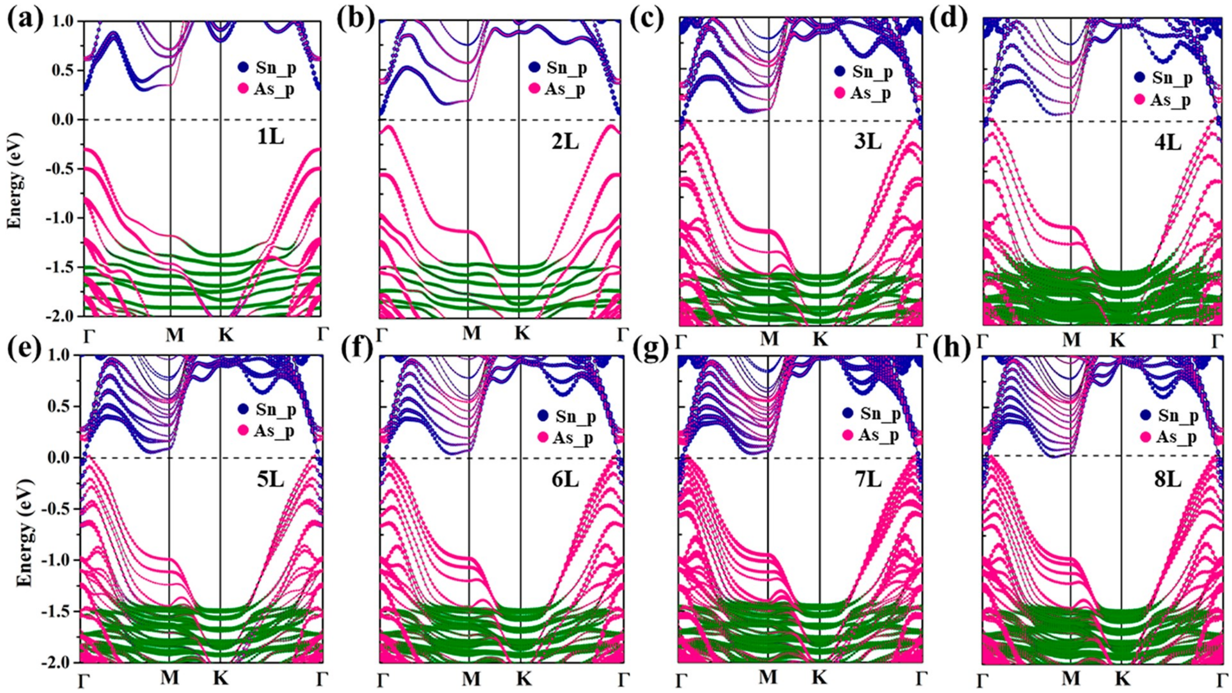

Figure 3. (a−h) Atom-resolved electronic band structures of $EnSn_2As_2$ with different layers. SOC is included in the calculations.

indicating its excellent thermal stability (Figure S1b,c). We further substantiate the mechanical stability of $EnSn_2As_2$ monolayer by calculating elastic constants with the finite distortion method. As listed in Table S1, the two independent elastic constants are C_{11} = 59.82 N/m and C_{12} = 15.99 N/m, and fully satisfy the Born−Huang criteria[45] of mechanical stability: $C_{11}C_{22} - C_{12}^2 > 0$ and $C_{66} > 0$, demonstrating that the $EnSn_2As_2$ monolayer is also mechanically stable. Compared to many established 2D materials, such as graphene (∼335 N/m),[46] MoS_2 (∼123 N/m),[47] and h-BN (∼267 N/m),[48] $EnSn_2As_2$ monolayer is very soft, but it is comparable with $MnSbBiTe_4$ monolayer (C_{11} = 75.79 N/m and C_{12} = 21.26 N/m).[49]

B. Magnetic and Electronic Properties of $EnSn_2As_2$ Monolayer. We next investigate the magnetic properties of the $EnSn_2As_2$ monolayer. To reveal the magnetic ground state, a 2 × 2 × 1 supercell with three magnetic configurations is constructed, including one FM and two AFM configurations (labeled as zigzag and stripe AFM, as shown in Figure S2). The calculated energy difference, ΔE, between AFM state and FM state ($E_{FM} - E_{AFM}$) as a function of Hubbard U are presented in Figure S3a. We find that although ΔE keeps decreasing with the increasing of Hubbard U (from 0 to 6 eV), the value is always negative, which indicates that the magnetic ground state of the $EnSn_2As_2$ monolayer is in FM configuration. This magnetic state is also robust against external strain (as shown in Figure S3b). The calculated magnetic moment is about 6.9 μ_B, which is contributed to by the seven unpaired f electrons of Eu^{2+} ions, as shown in the spin density results of Figure S4.

The calculated MAE of $EnSn_2As_2$ monolayer is shown in Figure 2a. Here the spin orientation is constrained in three different planes of *xy*, *xz*, and *yz*, respectively. The spin direction is presented by θ, which is defined as the angle between spin orientation and *x*-/*x*-/*z*-axis for the case of *xy*, *xz*, and *yz* planes, respectively. In total, the easy axis is along the (010) direction and the hard axis is along the (011) direction, and the corresponding MAE is 500 μeV/f.u., such a small magnetic anisotropy indicating a low Curie temperature. Indeed, the Curie temperature estimated by employing the MC simulations within the 2D Heisenberg model is 4.25 K, as shown in Figure 2b, which is comparable to 2D topological insulator $EuCd_2Bi_2$ (4 K)[50] and lower than those of FM $MnBi_2Te_4$ (20 K)[51] and CrI_3 (61 K).[52]

We further investigate the electronic band structures of the $EnSn_2As_2$ monolayer with in-plane FM configuration, as shown in Figure 2c. The calculated spin-polarized band structure without consideration of SOC indicates that the $EnSn_2As_2$ monolayer is a FM semiconductor with an indirect band gap of 0.63 eV. The valence band maximum (VBM) and conduction band minimum (CBM) are all contributed to by the spin-up states. The atom-orbital-resolved band structure including of SOC is plotted in Figure 2d. We find that the indirect band gap slightly decreases to 0.60 eV. The Eu f bands are far away from the Fermi level, and the bands near the Fermi level are contributed to by the Sn/As p orbitals. The band gap is so large that the VBM and CBM cannot be inverted, indicating the $EnSn_2As_2$ monolayer is topologically trivial. It should be noted that around the energy of −1.5 eV below Fermi level, the local Eu f electrons hybridize with itinerant As p and Sn p electrons. Such a hybridization can be used to manipulate the electronic properties via external magnetic field as demonstrated in the following.

In Figure 2d,e, we show the calculated electronic band structures of the $EnSn_2As_2$ monolayer with spin orientation along the easy axis (010) direction and the hard axis (011) direction, respectively. The VBM bands around the Γ point disperse quite slightly, and the CBM at Γ and Γ−M also have similar energy. With a careful check as shown in the zoomed-in pictures, we find that the VBM locates at the Γ point for both cases, while the CBM differs. In the case of the (010) direction, the CBM locates between Γ and M, resulting in an indirect band gap semiconductor with a band gap of 0.60 eV. When rotating the spin orientation to the (011) direction, the CBM location changes to the Γ point, so that the $EnSn_2As_2$

https://doi.org/10.1021/acsaelm.2c00414
ACS Appl. Electron. Mater. 2022, 4, 3212−3219

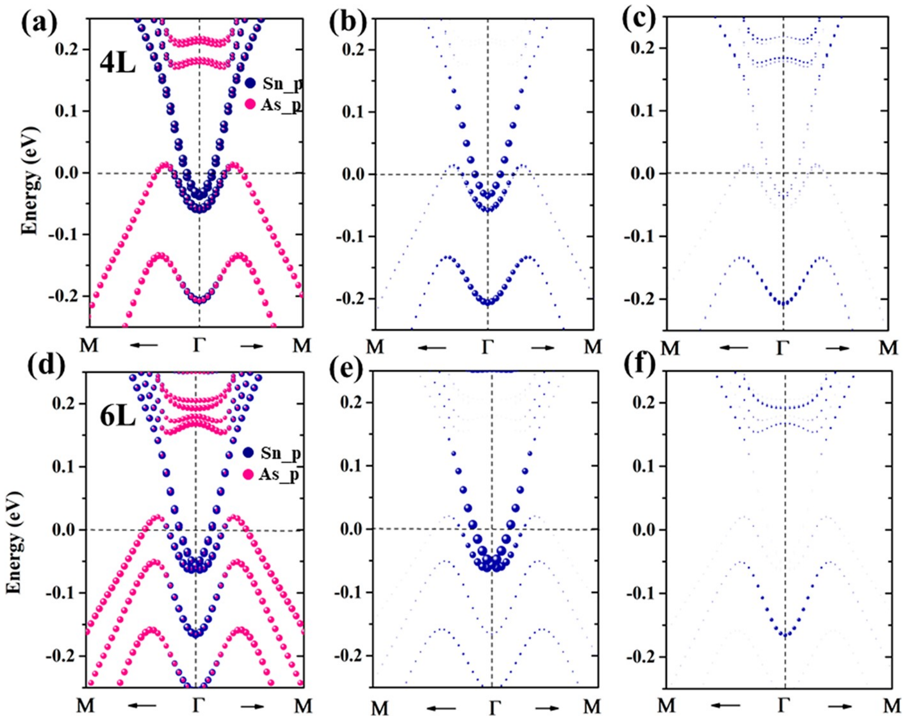

Figure 4. Zoomed-in atom-resolved electronic band structures of $EnSn_2As_2$ with (a) 4L and (d) 6L. The band contribution of surface Sn atoms and intermediate Sn atoms of (b, c) 4L and (e, f) 6L, respectively.

monolayer transforms to a direct band gap semiconductor with a band gap of 0.52 eV. We should note that the CBM energy difference between Γ and M′ (along Γ−M) is rather small for both of these cases: it is 3.6 meV for the (010) case and 6.21 meV for the (011) case. In addition, we find another significant change occurs at the Γ point with the energy of −0.75 eV below the Fermi level (highlighted in the red circle) and that the bands split about 157 meV in the (011) case, while such a split is absent in the case of the (010) spin orientation (see details in Figure S5). It is consistent with the spin textured band effect reported in CrI_3,[14] LaCl,[15] the $CoGa_2X_4$ (X = S, Se, or Te) family,[53] $EuTe_2$,[54] and the $Mn_3Si_2Te_6$ system.[55] A further discussion of spin textured band effect in $EnSn_2As_2$ will be given in the next section.

C. Electronic and Topological Properties of $EnSn_2As_2$ Multilayers. As discussed above, the $EuSn_2As_2$ monolayer is in in-plane FM order. While increasing the thickness of $EuSn_2As_2$ to bilayer or more, the intralayer AFM with in-plane spin orientation is still kept for most of the cases. While for some cases, e.g., 5L and 8L, the small MAE highly depends on the structure difference and calculation details and the out-of-plane easy axis might appear in the same calculation scheme (see Table 1 and Table S2). Here, to understand the effect of thickness and magnetic order on electronic structures, the evolution of the electronic band structures of $EuSn_2As_2$ with in-plane spin orientation from 1L to 8L is calculated. As shown in Figure 3, the $EuSn_2As_2$ monolayer and bilayer are indirect band gap semiconductors with gaps of 0.60 and 0.13 eV, respectively. For the ones with thickness larger than 3L, the band gap dismisses and metallic behavior emerges. The band near the Fermi level is contributed to by As p and Sn p orbitals, and the band inversion between these two kinds of orbitals occurs when the thickness increases to 4L or more, which indicates that a nontrivial surface state emerges.

To further confirm the existence of the nontrivial surface state, we carefully analyze the electronic band structures of 4L and 6L. Panels a and d of Figure 4 present the zoomed-in orbital projected band structures of 4L and 6L along the M−Γ−M high symmetry lines, in which around the Γ point the band inversion between As p valence band and Sn p conduction band appears. On the basis of this inversion mechanism, there also exists the linear band connecting conduction band to valence band that realizes the nontrivial surface state by comparing the surface and bulk Sn p orbital projection, as shown in panels b,c and e,f of Figure 4. It is also known that this nontrivial surface state originates from the topological insulator of bulk $EuSn_2As_2$.[33] Meanwhile, with an increase of layer number, there exists linear Dirac crossing points at the Γ points, which is in good agreement with experimental ARPES results.[33] Therefore, on the basis of our slab models, the topological properties of $EuSn_2As_2$ are verified again.

To analyze the effect of spin order on these nontrivial surface states, we then investigate the band structures of $EuSn_2As_2$ with different magnetic configurations. The giant variation of the band structure following the change of magnetic order, i.e., the spin textured band effect, requires three prerequisites: (1) strong spin−orbital coupling, (2) high magnetic crystalline anisotropy, and (3) collective magnetic behaviors. For $EuSn_2As_2$, both Eu f and As p orbitals display strong spin−orbital coupling and layered structure induces the giant crystalline anisotropy. Meanwhile, rare-earth Eu f orbital owns a strong magnetic coupling and a high saturated localized magnetic moment of 6.9 μ_B, which directly hybridizes with As p orbital. On the basis of these conditions, changing the direction of external magnetic field tunes the spin orientation of Eu f electrons and then can result in a significant change of As p electronic band structures due to their hybridization, i.e., the appearance of spin textured band effect in $EuSn_2As_2$. As

https://doi.org/10.1021/acsaelm.2c00414
ACS Appl. Electron. Mater. 2022, 4, 3212−3219

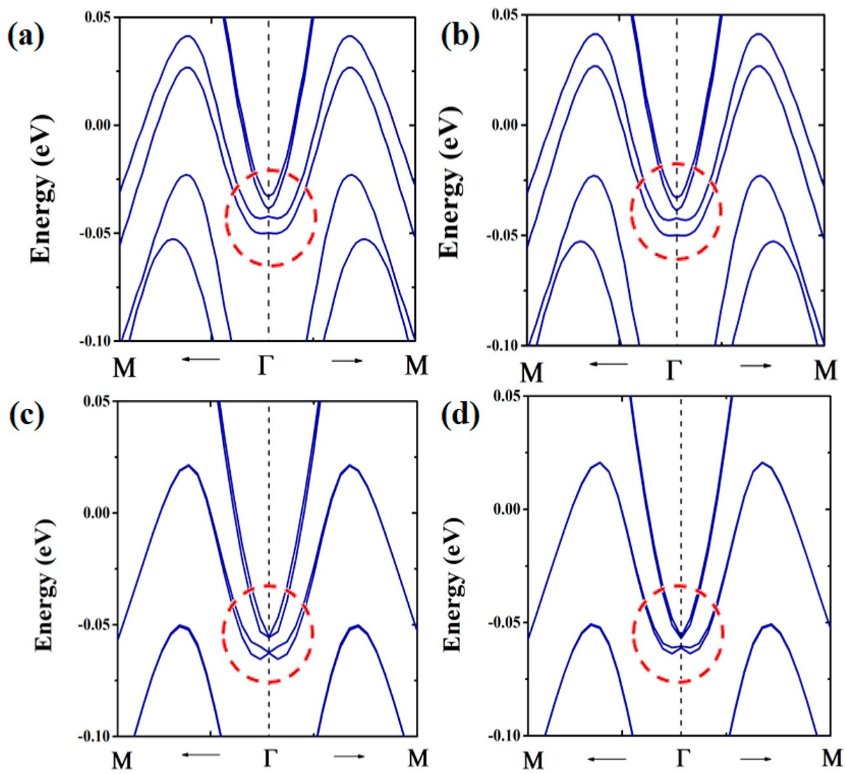

Figure 5. Band structures of 6L $EuSn_2As_2$ with different magnetic configurations. (a) FM-*z*, (b) FM-*x*, (c) AFM-*z*, and (d) AFM-*x*, respectively.

shown in Figure 5, the two highest valence bands of 6L for FM-*x* (FM configuration with spin orientation along the *x* direction) and FM-*z* orders have a huge spin splitting, but they are degenerate for AFM-*x* and AFM-*z* orders. Although time-reversal symmetry is broken for all of these magnetic orders, AFM states can keep some extent symmetry of mirror M_z symmetry, which reduces the spin splitting. Interestingly, surface states from Sn p orbital present almost degenerate energy levels especially close to the Γ point. The reason is that As atoms locate much closer with middle layer Eu atoms and block the effect of Eu; hence, the effect of Eu on the much further Sn atoms is significantly reduced. Therefore, spin splitting of Sn p and As p orbitals around the Fermi energy show two different features that band splitting of Sn p orbitals is small while that of As p orbitals is huge. Moreover, due to time-reversal symmetry even for combined symmetry (time-reversal symmetry with half-translation) breaking, there exists gaped Dirac surface states around Γ point. Finally, in combination of linear Dirac bands and spin-splitting features, layered $EuSn_2As_2$ provides a novel platform toward exploring the exotic topological properties as well as designing spintronic device.

■ CONCLUSIONS

In summary, the rare-earth 2D $EuSn_2As_2$ films, from 1L to 8L, were systematically investigated using first-principles calculations approach. The thickness-dependent structure and magnetic, electronic, and topological states are discussed in detail. Our results reveal that exfoliating the $EuSn_2As_2$ layers should be possible because of their small cleavage energy. The $EuSn_2As_2$ monolayer shows a soft structure as compared to many other 2D ultrathin structures and is an in-plane FM semiconductor with a band gap of 0.60 eV. The band gap can be transformed from an indirect to a direct one when spin orientation is changed from in-plane to out-of-plane. Moreover, interlayer AFM order appears in bilayer and thick layers. Increasing the layers to three, the electronic phase transition also occurs which it transforms from semiconductor in bilayer to metal in 3L. For thicker layers, the bands of Sn p and As p orbitals reverse and the nontrivial surface states emerge, which can be tuned to Dirac surface state by varying the spin direction of Eu. Our work demonstrates the thickness-dependent magnetism and electronic properties in $EuSn_2As_2$ and also brings a new material with a giant spin textured band effect. Our finding will provide an effective magnetism and topology tuning strategy in vdW layered materials.

■ ASSOCIATED CONTENT

Supporting Information

The Supporting Information is available free of charge at https://pubs.acs.org/doi/10.1021/acsaelm.2c00414.

Exfoliation energy, AIMD simulations and electronic localization (ELF); scheme of three different magnetic configurations energy differences between FM state and AFM states; spin density results; change of splitting energy and band gap with respect to the magnetic direction changes; total energy and elastic constants (PDF)

■ AUTHOR INFORMATION

Corresponding Authors

Peiheng Jiang − *CAS Key Laboratory of Magnetic Materials and Devices & Zhejiang Province Key Laboratory of Magnetic Materials and Application Technology, Ningbo Institute of Materials Technology and Engineering, Chinese Academy of Sciences, Ningbo 315201, China*;
Email: jiangph@nimte.ac.cn

Zhicheng Zhong − *CAS Key Laboratory of Magnetic Materials and Devices & Zhejiang Province Key Laboratory of Magnetic Materials and Application Technology, Ningbo Institute of Materials Technology and Engineering, Chinese Academy of Sciences, Ningbo 315201, China; China Center of Materials Science and Optoelectronics Engineering, University of Chinese Academy of Sciences, Beijing 100049, China;* orcid.org/0000-0003-1507-4814; Email: zhong@nimte.ac.cn

Authors

Xiaodong Lv − *Ganjiang Innovation Academy, Chinese Academy of Sciences, Ganzhou 341000, China; CAS Key Laboratory of Magnetic Materials and Devices & Zhejiang Province Key Laboratory of Magnetic Materials and Application Technology, Ningbo Institute of Materials Technology and Engineering, Chinese Academy of Sciences, Ningbo 315201, China*

Xuejiao Chen − *CAS Key Laboratory of Magnetic Materials and Devices & Zhejiang Province Key Laboratory of Magnetic Materials and Application Technology, Ningbo Institute of Materials Technology and Engineering, Chinese Academy of Sciences, Ningbo 315201, China*

Bingwen Zhang − *Fujian Key Laboratory of Functional Marine Sensing Materials, Minjiang University, Fuzhou 350108, China;* orcid.org/0000-0002-1655-2083

Complete contact information is available at:
https://pubs.acs.org/10.1021/acsaelm.2c00414

Author Contributions

[⊥]X.L. and X.C. contributed equally to this work.

Notes

The authors declare no competing financial interest.

■ ACKNOWLEDGMENTS

We acknowledge financial support from the National Key R&D Program of China (Grant Nos. 2021YFA0718900, and 2017YFA0303602), the Key Research Program of Frontier Sciences of CAS (Grant No. ZDBS-LY-SLH008), the National Nature Science Foundation of China (Grant No. 11974365), the Science Center of the National Science Foundation of China (Grant Nos. 52088101 and 51931011), K. C. Wong Education Foundation (Grant No. GJTD-2020-11), the Key Research Program of the Chinese Academy of Sciences (Grant No. ZDRW-CN-2021-3), Self-Deployed Projects of Ganjiang Innovation Academy, Chinese Academy of Sciences (Grant No. E055B002), and Ningbo Natural Science Foundation (Grant No. 202003N4363). The calculations are performed at the Supercomputing Center of Ningbo Institute of Materials Technology and Engineering.

■ REFERENCES

(1) Tang, P.; Zhou, Q.; Xu, G.; Zhang, S.-C. Dirac Fermions in an Antiferromagnetic Semimetal. *Nat. Phys.* **2016**, *12*, 1100−1104.

(2) Hua, G.; Nie, S.; Song, Z.; Yu, R.; Xu, G.; Yao, K. Dirac Semimetal in Type-IV Magnetic Space Groups. *Phys. Rev. B* **2018**, *98*, 201116.

(3) Xie, B.; Wang, H.-X.; Zhang, X.; Zhan, P.; Jiang, J.-H.; Lu, M.; Chen, Y. Higher-order Band Topology. *Nat. Rev. Phys.* **2021**, *3*, 520−532.

(4) Mong, R. S. K.; Essin, A. M.; Moore, J. E. Antiferromagnetic Topological Insulators. *Phys. Rev. B* **2010**, *81*, 245209.

(5) Otrokov, M. M.; Klimovskikh, I. I.; Bentmann, H.; Estyunin, D.; Zeugner, A.; Aliev, Z. S.; Gaß, S.; Wolter, A. U. B.; Koroleva, A. V.; Shikin, A.; Blanco-Rey, M.; Hoffmann, M.; Rusinov, I.; Vyazovskaya, A.; Eremeev, S.; Koroteev, Y.; Kuznetsov, V.; Freyse, F.; Sanchez-Barriga, L.; Amiraslanov, I.; Babanly, M.; Mamedov, N.; Abdullayev, N.; Zverev, V.; Alfonsov, A.; Kataev, V.; Büchner, B.; Schwier, E.; Kumar, S.; Kimura, A.; Petaccia, L.; Di Santo, G.; Vidal, R.; Schatz, S.; Kißner, K.; Ünzelmann, M.; Min, C.; Moser, S.; Peixoto, T.; Reinert, F.; Ernst, A.; Echenique, P.; Isaeva, A.; Chulkov, E. Prediction and Observation of an Antiferromagnetic Topological Insulator. *Nature* **2019**, *576*, 416−422.

(6) Baltz, V.; Manchon, A.; Tsoi, M.; Moriyama, T.; Ono, T.; Tserkovnyak, Y. Antiferromagnetic Spintronics. *Rev. Mod. Phys.* **2018**, *90*, 015005.

(7) Xu, Y. F.; Elcoro, L.; Song, Z. D.; Wieder, J. B.; Vergniory, M. G.; Regnault, N.; Chen, Y. L.; Felser, C.; Bernevig, B. A. High-throughput Calculations of Magnetic Topological Materials. *Nature* **2020**, *586*, 702−707.

(8) Elcoro, L.; Wieder, B. J.; Song, Z.; Xu, Y.; Bradlyn, B.; Bernevig, B. A. Magnetic Topological Quantum Chemistry. *Nat. Commun.* **2021**, *12*, 5965.

(9) Watanabe, H.; Po, H. C.; Vishwanath, A. Structure and Topology of Band Structures in the 1651 Magnetic Space Groups. *Sci. Adv.* **2018**, *4*, eaat8685.

(10) Li, J.; Li, Y.; Du, S.; Wang, Z.; Gu, B.-L.; Zhang, S.-C.; He, K.; Duan, W.; Xu, Y. Intrinsic Magnetic Topological Insulator in van der Waals Layered $MnBi_2Te_4$-family Materials. *Sci. Adv.* **2019**, *5*, eaaw5685.

(11) Zhang, Y.; Sun, Y.; Yang, H.; Železný, J.; Parkin, S. P. P.; Felser, C.; Yan, B. Strong Anisotropic Anomalous Hall Effect and Spin Hall Effect in the Chiral Antiferromagnetic Compounds Mn_3X (X = Ge, Sn, Ga, Ir, Rh, and Pt). *Phys. Rev. B* **2017**, *95*, 075128.

(12) Wang, Z.; Vergniory, M. G.; Kushwaha, S.; Hirschberger, M.; Chulkov, E. V.; Ernst, A.; Ong, N. P.; Cava, R. J.; Bernevig, B. A. Time-reversal Breaking Weyl Fermions in Magnetic Heusler Alloys. *Phys. Rev. Lett.* **2016**, *117*, 236401.

(13) Wang, Q.; Xu, Y.; Lou, R.; Liu, Z.; Li, M.; Huang, Y.; Shen, D.; Weng, H.; Wang, S.; Lei, H. Large Intrinsic Anomalous Hall Effect in Half-metallic Ferromagnet $Co_3Sn_2S_2$ with Magnetic Weyl Fermions. *Nat. Commun.* **2018**, *9*, 3681.

(14) Jiang, P. H.; Li, L.; Liao, Z.; Zhao, Y. X.; Zhong, Z. C. Spin Direction-controlled Electronic Band Structures in Two-dimensional Ferromagnetic CrI_3. *Nano Lett.* **2018**, *18*, 3844−3849.

(15) Liu, Z.; Zhao, G.; Liu, B.; Wang, Z. F.; Yang, J.; Liu, F. Intrinsic Quantum Anomalous Hall Effect with In-Plane Magnetization: Searching Rule and Material Prediction. *Phys. Rev. Lett.* **2018**, *121*, 246401.

(16) Zhang, Z.; Gao, Q.; Liu, C.-C.; Zhang, H.; Yao, Y. Magnetization-direction Tunable Nodal-line and Weyl phases. *Phys. Rev. B* **2018**, *98*, 121103.

(17) Zhang, B.; Sun, J.; Leng, J.; Zhang, C.; Wang, J. Tunable Two Dimensional Ferromagnetic Topological Half-metal CrO_2 by Electronic Correction and Spin Direction. *Appl. Phys. Lett.* **2020**, *117*, 222407.

(18) Chen, B.; Fei, F.; Zhang, D.; Zhang, B.; Liu, W.; Zhang, S.; Wang, P.; Wei, B.; Zhang, Y.; Zuo, Z.; Guo, J.; Liu, Q.; Wang, Z.; Wu, X.; Zong, J.; Xie, X.; Chen, W.; Sun, Z.; Wang, S.; Zhang, Y.; Zhang, M.; Wang, X.; Song, F.; Zhang, H.; Shen, D.; Wang, B. Intrinsic Magnetic Topological Insulator Phases in the Sb Doped $MnBi_2Te_4$ Bulks and Thin Flakes. *Nat. Commun.* **2019**, *10*, 4469.

(19) Kim, H. S.; Kim, C. H.; Jeong, H.; Jin, H.; Yu, J. Strain-induced Topological Insulator Phase and Effective Magnetic Interaction in Li_2IrO_3. *Phys. Rev. B* **2013**, *87*, 165117.

(20) Otrokov, M. M.; Rusinov, I. P.; Blanco-Rey, M.; Hoffmann, M.; Vyazovskaya, A.; Eremeev, S. A.; Ernst, A.; Echenique, P. M.; Arnau, A.; Chulkov, E. V. Uniqe Thickness-dependent Properties of the van der Waals Interlayer Antiferromagnetic $MnBi_2Te_4$. *Phys. Rev. Lett.* **2019**, *122*, 107202.

(21) Zhang, D.; Shi, M.; Zhu, T.; Xing, D.; Zhang, H.; Wang, J. Topological Axion States in the Magnetic Insulator $MnBi_2Te_4$ with the Quantized Magnetoelectric Effect. *Phys. Rev. Lett.* **2019**, *122*, 206401.
(22) Li, J.; Wang, C.; Zhang, Z.; Gu, B. L.; Duan, W.; Xu, Y. Magnetically Controllable Topological Quantum Phase Transitions in Antiferromagnetic Topological Insulator $MnBi_2Te_4$. *Phys. Rev. B* **2019**, *100*, 121103.
(23) Zhang, Y.; Yin, Y.; Dubuis, G.; Butler, T.; Medhekar, N.; Granville, S. Berry Curvature Origin of Thickness-dependent Anomalous Hall Effect in a Ferromagnetic Weyl Semimetal. *npj Quantum Mater.* **2021**, *6*, 17.
(24) Li, H.; Wang, H.; Gao, W.; Chen, Z.; Han, Y.; Zhu, X.; Tian, M. Thickness Dependence of Superconductivity in Layered Topological Superconductor β-$PdBi_2$. *Nanomaterials.* **2021**, *11*, 2826.
(25) Gao, P.; Li, X.; Yang, J. Thickness-dependent Magnetic Transition in Few Lyer 1T Phase $CrTe_2$. *J. Phys. Chem. Lett.* **2021**, *12* (29), 6847−6851.
(26) Yan, J.; Jiang, Z. Z.; Xiao, R. C.; Lu, W. J.; Song, W. H.; Zhu, X. B.; Luo, X.; Sun, Y. P.; Yamashita, M. Field-Induced Topological Hall Effect in Antiferromagnetic Axion Insulator Candidate $EuIn_2As_2$. *Phys. Rev. Res.* **2022**, *4*, 013163.
(27) Riberolles, S.; Trevisan, T.; Kuthanazhi, B.; Heitmann, T.; Ye, F.; Johnston, D.; Bud'ko, S.; Ryan, D.; Canfield, P.; Kreyssig, A.; Vishwanath, A.; McQueeney, R.; Wang, L.-L.; Orth, P.; Ueland, B. Magnetic Crystalline-Symmetry-Protected Axion Electrodynamics and Field-Tunable Unpinned Dirac Cones in $EuIn_2As_2$. *Nat. Commun.* **2021**, *12*, 999.
(28) Arguilla, M. Q.; Cultrara, N. D.; Baum, Z. J.; Jiang, S.; Ross, R. D.; Goldberger, J. E. $EuSn_2As_2$: An Exfoliatable Magnetic Layered Zintl-klemm Phase. *Inorg. Chem. Front.* **2017**, *4*, 378.
(29) Gui, X.; Pletikosic, I.; Cao, H.; Tien, H.-J.; Xu, X.; Zhong, R.; Wang, G.; Chang, T.-R.; Jia, S.; Valla, T.; Xie, W.; Cava, R. J. A New Magnetic Topological Quantum Material Candidate by Design. *ACS Cent. Sci.* **2019**, *5*, 900−910.
(30) Sun, H.; Chen, C.; Hou, Y.; Wang, W.; Gong, Y.; Huo, M.; Li, L.; Yu, J.; Cai, W.; Liu, N.; Wu, R.; Yao, D.; Wang, M. Magnetism Variation of the Compressed Antiferromagnetic Topological Insulator $EuSn_2As_2$. *Sci. China Phys. Mech. Astron.* **2021**, *64*, 118211.
(31) Pakhira, S.; Tanatar, M. A.; Heitmann, T.; Vaknin, D.; Johnston, D. C. A-type Antiferromagnetic Order and Magnetic Phase Diagram of the Trigonal Eu spin-7/2 Triangular-lattice Compound $EuSn_2As_2$. *Phys. Rev. B* **2021**, *104*, 174427.
(32) Li, H.; Gao, W.; Chen, Z.; Chu, W.; Nie, Y.; Ma, S.; Han, Y.; Wu, M.; Li, T.; Niu, Q.; Ning, W.; Zhu, X.; Tian, M. Magnetic Properties of the Layered Magnetic Topological Insulator $EuSn_2As_2$. *Phys. Rev. B* **2021**, *104*, 054435.
(33) Li, H.; Gao, S.-Y.; Duan, S.-F.; Xu, Y.-F.; Zhu, K.-J.; Tian, S.-J.; Gao, J.-C.; Fan, W.-H.; Rao, Z.-C.; Hugang, J.-R.; Li, J.-J.; Yan, D.-Y.; Liu, Z.-T.; Liu, W.-L.; Huang, Y.- B.; Li, Y.-L.; Liu, Y.; Zhang, G.-B.; Zhang, P.; Kondo, T.; Shin, S.; Lei, H.-C.; Shi, Y.-G.; Zhang, W.-T.; Weng, H.- M.; Qian, T.; Ding, H. Dirac Surface States in Intrinsic Magnetic Topological Insulators $EuSn_2As_2$ and $MnBi_{2n}Te_{3n+1}$. *Phys. Rev. X* **2019**, *9*, 041039.
(34) Kresse, G.; Furthmüller, J. Efficient Iterative Schemes for *ab initio* Total-energy Calculations Using a Plane-wave Basis Set. *Phys. Rev. B* **1996**, *54*, 11169−11186.
(35) Perdew, J. P.; Burke, K.; Ernzerhof, M. Generalized Gradient Approximation Made Simple. *Phys. Rev. Lett.* **1996**, *77*, 3865−3868.
(36) Kresse, G.; Joubert, D. From Ultrasoft Pseudopotentials to the Projector Augmented-wave Method. *Phys. Rev. B* **1999**, *59*, 1758.
(37) Bučko, T.; Hafner, J.; Lebègue, S.; Ángyán, J. G. Improved Description of the Structure of Molecular and Layered Crystals: *ab initio* DFT Calculations with van der Waals Corrections. *J. Phys. Chem. A* **2010**, *114*, 11814−11824.
(38) Monkhorst, H. J.; Pack, J. D. Special Points for Brillouin-zone Integrations. *Phys. Rev. B* **1976**, *13*, 5188−5192.
(39) Dudarev, S.; Botton, G.; Savrasov, S.; Humphreys, C.; Sutton, A. Electron-energy-loss Spectra and the Structural Stability of Nickel Oxide: an LSDA+ U Study. *Phys. Rev. B* **1998**, *57*, 1505.
(40) Togo, A.; Tanaka, I. First Principles Phonon Calculation in Material Science. *Scr. Mater.* **2015**, *108*, 1−5.
(41) Martyna, G. J.; Klein, M. L.; Tuckerman, M. E. Nosé−Hoover Chains: The Canonical Ensemble Via Continuous Dynamics. *J. Chem. Phys.* **1992**, *97*, 2635.
(42) Liu, L.; Ren, X.; Xie, J.; Cheng, B.; Liu, W.; An, T.; Qin, H.; Hu, J. Magnetic Switches Via Electric Field in BN Nanoribbons. *Appl. Surf. Sci.* **2019**, *480*, 300−307.
(43) Xiang, H.; Lee, C.; Koo, H.-J.; Gong, X.; Whangbo, M.-H. Magnetic Properties and Energy Mapping Analysis. *Dalton Trans.* **2013**, *42*, 823−853.
(44) Björkman, T.; Gulans, A.; Krasheninnikov, A. V.; Nieminen, R. M. van der Waals Bonding in Layered Compounds from Advanced Density-functional First-principles Calculations. *Phys. Rev. Lett.* **2012**, *108*, 235502.
(45) Wang, J.; Yip, S.; Phillpot, S. R.; Wolf, D. Crystal Instability at Finite Strain. *Phys. Rev. Lett.* **1993**, *71*, 4182−4185.
(46) Topsakal, M.; Cahangirov, S.; Ciraci, S. The Response of Mechanical and Electronic Properties of Graphane to the Elastic Strain. *Appl. Phys. Lett.* **2010**, *96*, 091912.
(47) Yue, Q.; Kang, J.; Shao, Z.; Zhang, X.; Chang, S.; Wang, G.; Qin, S.; Li, J. Mechanical and Electronic Properties of Monolayer MoS_2 under Elastic Strain. *Phys. Lett. A* **2012**, *376*, 1166−1170.
(48) Peng, Q.; Ji, W.; De, S. Mechanical Properties of the Hexagonal Boron Nitride Monolayer: Ab Initio Study. *Comput. Mater. Sci.* **2012**, *56*, 11−17.
(49) Guo, S. D.; Wang, M. X. Predicted Intrinsic Piezoelectric Ferromagnetism in Janus Monolayer $MnSbBiTe_4$: a First Principles Study. *Phys. Chem. Chem. Phys.* **2021**, *23*, 22443−22450.
(50) Wang, H.; Mao, N.; Hu, X.; Dai, Y.; Huang, B.; Niu, C. W. A Magnetic Topological Insulator in Two-dimensional $EuCd_2Bi_2$: Giant Gap with Robust Topology against Magnetic Transitions. *Mater. Horiz.* **2021**, *8*, 956−961.
(51) Li, Y.; Jiang, Z.; Li, J.; Xu, S.; Duan, W. Magnetic Anisotropy of the Two-dimensional Ferromagnetic Insulator $MnBi_2Te_4$. *Phys. Rev. B* **2019**, *100*, 134438.
(52) McGuire, M. A.; Dixit, H.; Cooper, V. R.; Sales, C. B. Coupling of Crystal Structure and Magnetism in the Layered Ferromagnetic Insulator CrI_3. *Chem. Mater.* **2015**, *27* (2), 612−620.
(53) Zhang, S.; Xu, R.; Duan, W.; Zou, X. Intrinsic Half-metallicity in 2D Ternary Chalcogenides with High Critical Temperature and Controllable Magnetization Direction. *Adv. Funct. Mater.* **2019**, *29*, 1808380.
(54) Yang, H.; Liu, Q.; Liao, Z.; Si, L.; Jiang, P.; Liu, X.; Guo, Y.; Yin, J.; Wang, M.; Sheng, Z.; Zhao, Y.; Wang, Z.; Zhong, Z.; Li, R.-W. Colossal Angular Magnetoresistance in the Antiferromagnetic Semiconductor $EuTe_2$. *Phys. Rev. B* **2021**, *104*, 214419.
(55) Seo, J.; Seo, J.; De, C.; Ha, H.; Lee, J. E.; Park, S.; Park, J.; Skourski, Y.; Choi, E. S.; Kim, B.; Cho, G. Y.; Yeom, H. W.; Cheong, S.-W.; Kim, J. H.; Yang, B.-J.; Kim, K.; Kim, J. S. Colossal Angular Magnetoresistance in Ferrimagnetic Notal-Line Semiconductors. *Nature* **2021**, *599*, 576−581.